PAPER

A syndromic diagnostic assay on a macrochannel-to-digital microfluidic platform for automatic identification of multiple respiratory pathogens†

Cheng Dong,‡[a] Fei Li, [iD] ‡[bc] Yun Sun,[c] Dongling Long,[d] Chunzhao Chen,[e] Mengyan Li, [iD] [f] Tao Wei,[gh] Rui P. Martins,[i] Tianlan Chen*[c] and Pui-In Mak*[ij]

The worldwide COVID-19 pandemic has changed people's lives and the diagnostic landscape. The nucleic acid amplification test (NAT) as the gold standard for SARS-CoV-2 detection has been applied in containing its transmission. However, there remains a lack of an affordable on-site detection system at resource-limited areas. In this study, a low cost "sample-in-answer-out" system incorporating nucleic acid extraction, purification, and amplification was developed on a single macrochannel-to-digital microfluidic chip. The macrochannel fluidic subsystem worked as a world-to-chip interface receiving 500–1000 μL raw samples, which then underwent bead-based extraction and purification processes before being delivered to DMF. Electrodes actuate an eluent dispensed to eight independent droplets for reverse transcription quantitative polymerase chain reaction (RT-qPCR). By reading with 4 florescence channels, the system can accommodate a maximum of 32 detection targets. To evaluate the proposed platform, a comprehensive assessment was conducted on the microfluidic chip as well as its functional components (*i.e.*, extraction and amplification). The platform demonstrated a superior performance. In particular, using clinical specimens, the chip targeting SARS-CoV-2 and Flu A/B exhibited 100% agreement with off-chip diagnoses. Furthermore, the fabrication of chips is ready for scaled-up manufacturing and they are cost-effective for disposable use since they are assembled using a printed circuit board (PCB) and prefabricated blocks. Overall, the macrochannel-to-digital microfluidic platform coincides with the requirements of point-of-care testing (POCT) because of its advantages: low-cost, ease of use, comparable sensitivity and specificity, and availability for mass production.

[a] *School of Intelligent Systems Science and Engineering/JNU-Industry School of Artificial Intelligence, Jinan University, Zhuhai 519000, China*

[b] *Department of Biomedical Engineering, Jinan University, Guangzhou, 510632, China*

[c] *Digifluidic Biotech Ltd., Zhuhai 519000, China.*
E-mail: oscar.chen@digifluidic.com

[d] *Zhuhai Center for Disease Control and Prevention, Zhuhai 519087, China*

[e] *Advanced Interdisciplinary Institute of Environment and Ecology, Beijing Normal University, Zhu Hai 519087, China*

[f] *Department of Chemistry and Environmental Science, New Jersey Institute of Technology, Newark, 07102, USA*

[g] *Department of Bioengineering, College of Food Science, South China Agricultural University, Guangzhou, 510640, China*

[h] *Pan Asia (Jiangmen) Institute of Biological Engineering and Health, Jiangmen, 529080, China*

[i] *State-Key Laboratory of Analog and Mixed-Signal VLSI, Institute of Microelectronics, University of Macau, Taipa, Macau SAR, 999078, China.*
E-mail: pimak@um.edu.mo

[j] *Faculty of Science and Technology, University of Macau, Taipa, Macau SAR, 999078, China*

† Electronic supplementary information (ESI) available. See DOI: https://doi.org/10.1039/d3lc00728f

‡ These authors contributed equally to this work.

Introduction

The nucleic acid amplification test (NAT) is a technology that detects a particular deoxyribonucleic acid (DNA) or ribonucleic acid (RNA) sequence. It thus could sensitively and specifically[1] detect a few copies of a given nuclei acid with a small sample size. Various NAT technologies have long been used in many fields such as molecular research, genetic testing, forensics, agriculture and clinical medicine.[2] Among them, reverse transcription-quantitative PCR (RT-qPCR) has been widely accepted as the gold standard in many clinical diagnostics, such as detecting various pathogens in the respiratory tract, intestinal tract, and reproductive systems.[3,4] This is attributed to its well-recognized properties of quantification, sensitivity, and specificity.

The worldwide pandemic caused by severe acute respiratory syndrome coronavirus 2 (SARS-CoV-2) has significantly changed the daily lives of billions and deeply impacted global development in economic, political, and social domains. As an infectious respiratory virus, its main clinical manifestations were reported similar to influenza A/B

viruses and other common cold-induced bacteria/viruses, resulting in complicating the diagnosis of COVID-19 from symptoms.[5] Unfortunately, SARS-CoV-2 is potentially pre- or oligosymptomatically transmitted[6] and elicits relatively high community transmission (674 million cases) and mortality (6.8 million deaths).[7] Rapid diagnostic assays, therefore, are of urgent need for containing the spread of COVID-19 and/or other infectious diseases. Previous research reported that NAT could timely and easily detect pathogens from specimens such as nasopharyngeal and oropharyngeal swabs upon symptom onset.[8] However, several drawbacks still exist. It requires complex equipment in a centralized laboratory and highly skilled technicians to operate it. Meanwhile, this kind of offsite detection introduces many uncertainties regarding timeliness and safety. Thus, fully automatic equipment is imperative for decentralized use in source-limited regions.

Microfluidics is an eloquent technology for picoliter- to microliter-sized droplet manipulation. It has been applied in diverse decentralized NAT diagnoses which have been partially commercialized such as GeneXpert® from Cepheid, FilmArray® from BioFire Diagnosis, Cobas Liat® from Roche, *etc.* They are all fully automatic and portable point-of-care test (POCT) devices with self-contained, single use, biosafe, microfluidic cartridges for NATs. Digital microfluidics (DMF) based on electrowetting-on-dielectric (EWOD) provides an alternative for POCT devices and cartridges. This technology has been developed for over 40 years and is widely employed for multiple purposes.[9,10] Many researchers have developed their unique DMF devices for specific applications or cutting edge research goals, such as various omics sample preparation,[11–13] online monitoring of chemicals,[14] antimicrobial susceptibility test,[15] and even pollutant monitoring.[16] The DMF chip discretely actuates droplets on an array of electrodes without external pumps or valves or complicated geometries, and it can be simply fabricated by photolithography.[17] DMF, thus, is readily available for commercial use such as NAT, liberating tedious operations in the laboratory.[18] However, indeed, the development and commercialization of DMF are sluggish, which have been hindered by the gap between research and market.[18] Several companies (*e.g.*, Nanolytics, NuGEN, Advanced Liquid Logic) are dedicated to DMF commercialization mostly in the area of biomedical utilization. Successful products proved that DMF is a feasible tool for various biological applications; nevertheless, the failures of pioneering products such as NeoPrep Library Prep System by Illumina (famous for its sequencing equipment) remind us of the challenges of engineering and manufacturing.[19] Thus, many efforts were made to increase the reliability through the design of the circuitry,[20] optimization of reagents,[21,22] and other approaches.[23–25]

However, the feasibility of DMF technology in the field of qPCR nucleic acid detection remains to be verified due to challenges such as sample acceptance, seamless connection between extraction and amplification, and fluorescence detection. In the meantime, the scarcity of research into DMF commercialization also provided an impetus to propose this study, particularly with regard to the design of DMF chips. Herein, an all-in-one NAT system was presented, named Virus Hunter 2.0 (VH 2.0). This study aimed to provide insights into the diagnostic applications of DMF from its design and commercialization. Compared with the previous version VH 1.0, the following improvements were made to realize a "sample-in-to-result-out" fully automatic process: (1) VH 2.0 integrated automatic nucleic acid extraction process; (2) all reagents are stored in the chip through diverse approaches depending on their properties and forms; (3) the macrochannel-to-digital microfluidics is adopted. It served as a world-to-chip interface which receives hundreds of microliters of samples and exports a limited volume of liquid for DMF manipulation; specially designed electrodes for droplets overcome the height difference from macrochannel to digital microfluidics; (4) the thin-film heater on the chip is similar to a previous version because it provides an accurate temperature control and miniaturized device. In this version we improve the performance of the temperature control by changing the resistor's location and the geometry of the copper foil. Moreover, as a commercial product, the performance and reliability of the system have been strictly evaluated before mass production, including the performances of discrete modules, integrated chips, and clinical specimens and a wide variety of aspects. We also compared VH 2.0 with other POCT platforms targeting respiratory pathogens based on microfluidics. In summary, this study improved the automation and integration levels of a DMF-based nucleic acid detection platform, which brings the DMF technology significantly closer to commercialization.

Experimental

Reagents and materials

Pseudo-viruses of SARS-CoV-2 and influenza A/B with a concentration of 10^8 copies per mL were purchased from Sangon Biotech (Shanghai, China). Upon receipt, they were immediately aliquoted into 1.5 mL micro-centrifuge tubes and stored at −80 °C for future use. Primers and probes were designed to target the M1 gene from influenza A, the hemagglutinin gene from influenza B, and nucleocapsid protein and ORF1 genes from SARS-CoV-2 according to previous research[26] and synthesized by Sangon Biotech (Shanghai, China). Sequences are indicated in Table S1 in the ESI.† Magnetic beads and commercial pathogen nucleic acid extraction kits were purchased from EasyDiagnosis Co., Ltd. (Wuhan, China). All the other materials were purchased from Sangon Biotech (Shanghai, China) if not specifically indicated.

VH 2.0 system

VH 2.0 device. The illustration of the VH 2.0 device is shown in Fig. 1a with the dimensions of 330 mm × 250 mm
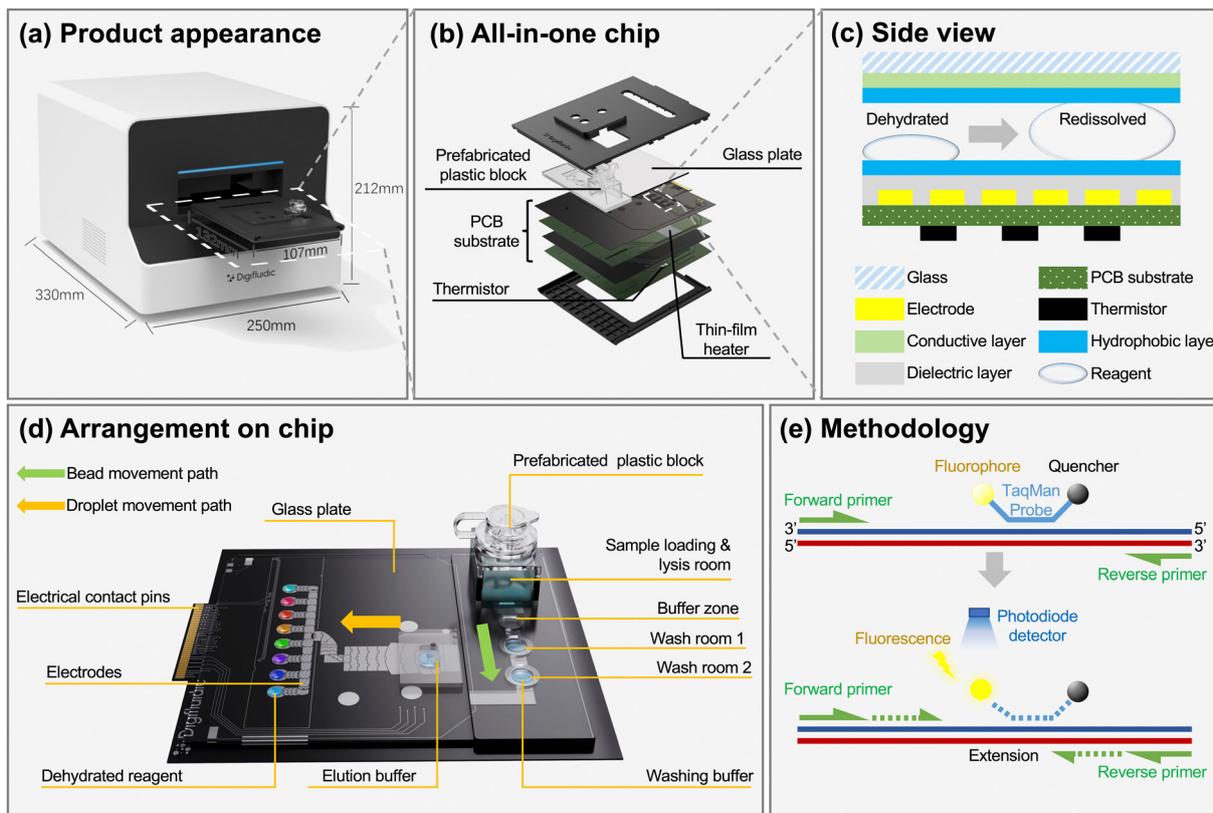
Fig. 1 (a) The product appearance of Virus Hunter 2.0 (VH 2.0) with dimensions. The chip based on digital microfluidic technology is framed by white dash lines and the tailored analysis device is also exhibited. (b) 3D explosive diagram of DMF chip, composed of top case, ITO-coated glass/prefabricated blocks, four-layer PCB (patterned with electrodes, thin-film heater, sensor), and bottom case, indicated from top to bottom in the figure. Part of the reaction points are framed by white dash lines. (c) The dehydrated and redissolved statuses of reagents at qPCR reaction sites. The stacked structure is presented in side view. (d) The arrangement of the VH 2.0 chip including key modules of extraction (*i.e.*, sample loading and lysis room, wash room 1 and 2, elution area) and amplification (*i.e.*, separation area and reaction points) parts. Prestored reagent allows "sample-in-to-answer-out" without additional pipetting. The movement paths of beads and droplet on the chip are indicated by green and orange arrows. (e) The schematic diagram of TaqMan qPCR chemistry on the chip. Briefly, the extension of primer enables the release of fluorophore and capture by the photodiode detector.

× 212 mm. It is composed of (1) a magnetic module – a motorized magnetic rod underneath the chip loading pocket is utilized to collect and attract beads, while two magnets generate a repulsive magnetic field for scattering beads in washing/eluting buffers; (2) a cooling system – benefits by the integration of a heating module on chip; the heating modules were removed from devices. Only a metal block with large specific heat capacity was implemented to achieve the maximal cooling rate of 5 °C s⁻¹; (3) an optical system – an arrangement of LEDs, filters, lenses, beam splitter, and photodiode was employed for fluorophore detection; (4) an electronic module – transformer and relay jointly control the switching and delivered voltage of the electrodes. Consequently, precise control of various droplets of different sizes can be achieved.

VH 2.0 chip design and fabrication. The VH 2.0 chip is 132 mm × 107 mm with the full function of detecting specific genes from pathogens. In addition to its routine functions, two innovations are implemented on tiny chips, which are (1) combination of channel-based microfluidics for nucleic acid extraction with digital microfluidics for RT-qPCR preparation

and reaction; (2) integration of the resistive thin-film heater and thermal sensor in printed circuit boards (PCBs). The introduction of channel-based microfluidics allows the handling of large volumes of buffers and magnetic beads in the nucleic acid extraction train. A sampling tube, lysis room, and two washing rooms were prefabricated with polycarbonate (PC) and liquid reagents were encapsulated at a specific room (Fig. 1d). At the digital microfluidic region, an indium tin oxide (ITO)-coated top glass was rigorously parallelized to the PCB with a consistent clearance (0.6 mm), forming a micro-chamber filled with mineral oil. As usual, an EWOD DMF chip and dielectric and conductive layers were applied to the upper side of the bottom plate. Then both surfaces were treated with hydrophobic material according to the method in a previous publication.[27] In detail, the surfaces were firstly cleaned with isopropanol and hydrophobically treated with FluoroPel PFC 1101V before baking (100 °C, 5 min), enabling droplets to move smoothly in the chamber. The prestored reagents for qPCR (*i.e.*, primers, probes, dNTP, enzymes) were dehydrated at the specific reaction room as shown in Fig. 1c. As a novel design extended to VH 2.0, the

thin-film heater and sensor were embedded in the four-layer PCB (Fig. 1b). Combined with a proportion integration differentiation (PID) controller, the chip could precisely control the temperature. Interestingly, note that the successfully commercialized digital microfluidic products have been mostly based on PCB substrates to date. This is most likely due to the mature production process, industrial chain, and excellent plasticity of PCB.

VH 2.0 control software design. The framework of the control software is shown in Fig. S1.† A graphic user interface (GUI) was developed for the visualization of device status and control. The embedded algorithm includes judgment of abnormal values, median filter, moving average filter, segment interpretation, and positive feature annotation. The cycle threshold (Ct) was computed using a well-recognized second derivative, which is defined as the fractional cycle where the second derivative of the real-time fluorescence intensity curve reaches the maximum value.[28] The detection results can be uploaded to a server and/or read instantly through multiple mobile terminals by Bluetooth.

System operation. Only three simple steps are requisite for VH 2.0 users: (1) add sample—shake the tube loaded with a pharyngeal swab 10–20 times and then add 500 µL of sample to the sample loading reservoir (maximal loading is 1000 µL) and cover the lid; (2) insert chip—insert the microchip into the device and start the analysis software; (3) read results—results are available after the analysis completion.

On-chip "sample-to-answer" workflow. The on-chip workflow was developed for sample RNA extraction and RT-qPCR processing (Fig. S2†). The detailed "sample-to-answer" procedure is as follows: (1) 500 µL of raw sample was injected into the sampling tube; (2) the injected sample pushed 20 µL and 5 µL proteinase K and magnetic beads into the lysis room; (3) the sample was mixed with 1000 µL lysis buffer and incubated at 60 °C for 2 min; (4) the released RNA bound to magnetic beads; (5) the magnet under the chip moved upward and collected the beads; (6) beads were drawn by magnet into wash room 1 and mixed with 90 µL wash buffer 1; (7) the binding RNA was subjected to a washing process together with the beads; (8) beads moved to wash room 2 and mixed with 90 µL wash buffer 2; (9) beads exerted wash procedure again; (10) beads moved to the next room; (11) the binding RNA was eluted from beads by 60 µL elution buffer at 60 °C; (12) beads were discarded; (13) the pure RNA moved to the separating area and (14) dispensed to 8 droplets of 5.55 µL per drop; (15) the dispensed droplets moved to the PCR region and redissolved with dried PCR premix; qPCR was performed in these units and the fluorescence signal was sent to the VH 2.0 analyzer. The chemistries are shown in Fig. 1e.

Validation of the VH 2.0 biochip performance

Validation of RNA extraction module. To compare the extraction efficiency between the VH 2.0 chip and off-chip manual extraction, samples containing 10^7 copies per mL of SARS-CoV-2 pseudo-virus were prepared and subjected to on-chip extraction using a bead based nucleic acid extract kit (EasyDiagnosis Biomedicine, Wuhan, China). The off-chip extraction process exactly followed the manufacturer's instructions. After extraction, 5 µL of the pure RNA in the elution buffer, as template, was added to 25 µL RT-qPCR reaction mixture containing 6.25 µL of qPCR mix, 2 µM of each forward and reverse primer, and 0.2 µM probe. Primers targeting N gene and ORF1 were the same as the prestored reagents listed in Table S1.† Then reactions were run with Gentier96 (Tianlong, Xian, China) following the temperature program: initially held at 50 °C for 15 min, then raised to 95 °C for 5 min, followed by 45 cycles of 10 s at 95 °C and 30 s at 60 °C.

Validation of amplification module. Off-chip qPCR validation was carried out with the total volume of 5 µL reaction mix to mimic the on-chip reaction in droplets. The qPCR reaction (5 µL) consists of 1 µL diluted RNA, 1.25 µL of 4× qPCR mix (same as the on-chip prestored reagents), 0.4 µM each forward and reverse primer, 0.2 µM probe and RNA/DNA-free water to a total volume of 5 µL. qPCR was run with Gentier96 following the same temperature program as previously. On-chip validation was carried out with integrated biochips. 60 µL of the target concentration of samples was added to the elution room and dispensed into 8 uniform droplets by EWOD force and then moved to chambers individually. The test samples were prepared by series diluted RNA extracted from pseudo-viruses and quantitated by qPCR with an existing standard curve. For comparison, the final copy numbers per test were designed as 300, 150, 75, 37.5, 15 for both off-chip and on-chip assays. At least duplicate chips were performed for each concentration. 4 replicates were run with off-chip qPCR. 20 off-chip repetitions were performed for the lowest concentration (i.e., 15 copies per test).

Evaluation of the integrated biochip. The pseudo-viruses with known concentrations were series diluted to designed targets for the validation of integrated chips. An estimation of the limit of detection (LOD) for each pathogen on the integrated chip was determined by testing at the tiers of 106, 105, 104, 103, 102, 10 copies per mL. Each test was processed in triplicate. The LOD is defined as the lowest amount of analyte that can be reliably detected, typically over 95% of the tested sample is supposed to be positive, namely LOD_{95}. It could be calculated by fitting apparent data with the probit regression curve according to the method provided by the Clinical and Laboratory Standards Institute (CLSI).[29] Operationally, the statistical software SPSS (v25, IBM) was adopted for running the algorithm. Linearity of the data was evaluated by fitting the logarithm of series concentrations against cycle thresholds with a linear regression model. Moreover, the qPCR efficiencies were calculated using the formula

$$\text{Efficiency} = 10^{-1/\text{slope}} - 1.$$

To determine the specificity of the integrated VH 2.0 chip, various pathogens besides SARS-CoV-2 and influenza A/B

virus were artificially spiked to preservation solution and run with chips. Tested pathogens were acquired from the Zhuhai Center for Disease Control and Prevention, including human parainfluenza virus (subtype HPIV1-4), human respiratory syncytial virus, human rhinoviruses, human adenovirus, *Streptococcus pneumoniae*, *Haemophilus influenzae*, *Staphylococcus aureus*, *Salmonella enterica*, and *Shigella flexneri*.

Validation with clinical specimens. To verify the diagnostic performance of the VH 2.0 in clinical applications, 22 positive samples and 6 negative samples were provided by the Zhuhai Center for Disease Control and Prevention. Among them, 11 samples were SARS-CoV-2 positive and 11 were Flu A; Flu B positive sample was not obtained during the time. All samples were collected by nasopharyngeal swabs and then placed in a commercially available sample preservation solution (Kunrongda, Shenzhen, China). The solution was divided into two portions for the following detection. One part was loaded into a VH 2.0 chip and the other portion was subjected to RNA extraction and RT-PCR in a certified biosafety level 2 laboratory. The off-chip qPCR reactions were conducted using the same reaction mixture as on-chip reactions. The correlation of the results (*i.e.*, Ct values) between on- and off-chip were evaluated by Pearson correlation coefficient (Pearson's *R*), and corresponding *p* values were obtained.

Stability assay of VH 2.0 biochips. Aiming to scale up the fabrication of the VH 2.0 biochip, a stability assay was conducted within a certain duration. To be specific, concentrations near the detection limits (*i.e.*, 1000 copies per mL for SARS-CoV-2(N) and Flu A/B and 100 copies per mL for SARS-CoV-2(ORF1)) were run with the same batch of products (chips and instrument) at an interval of one month. Each sample was tested with three chips.

Results and discussion

Temperature control

A uniplanar heater together with an NTC thermistor achieved rapid and accurate on-chip heating and sensing. By optimizing the resistor's pattern on the PCB and implementing PID control (Fig. 2c), it is possible to generate a homogenous temperature within the paralleled qPCR reaction spots at a relatively short response reaching an asymptotic state (90% of the set temperature). That was about 13 s drop from 95 °C to 60 °C and took about 4 s raising up to 95 °C (Fig. 2a). At the asymptotic state, fine adjustments were made to approach the set temperature and then retained at the setpoint. Temperatures fluctuated with $<\pm 1.27$ °C (2.11% of the set temperature) at the conditioning period (the first few seconds upon set temperature) and $<\pm 0.5$ °C (0.49% of the set temperature) at the stable period (Fig. 2a and b). As heat was lost at the edge of
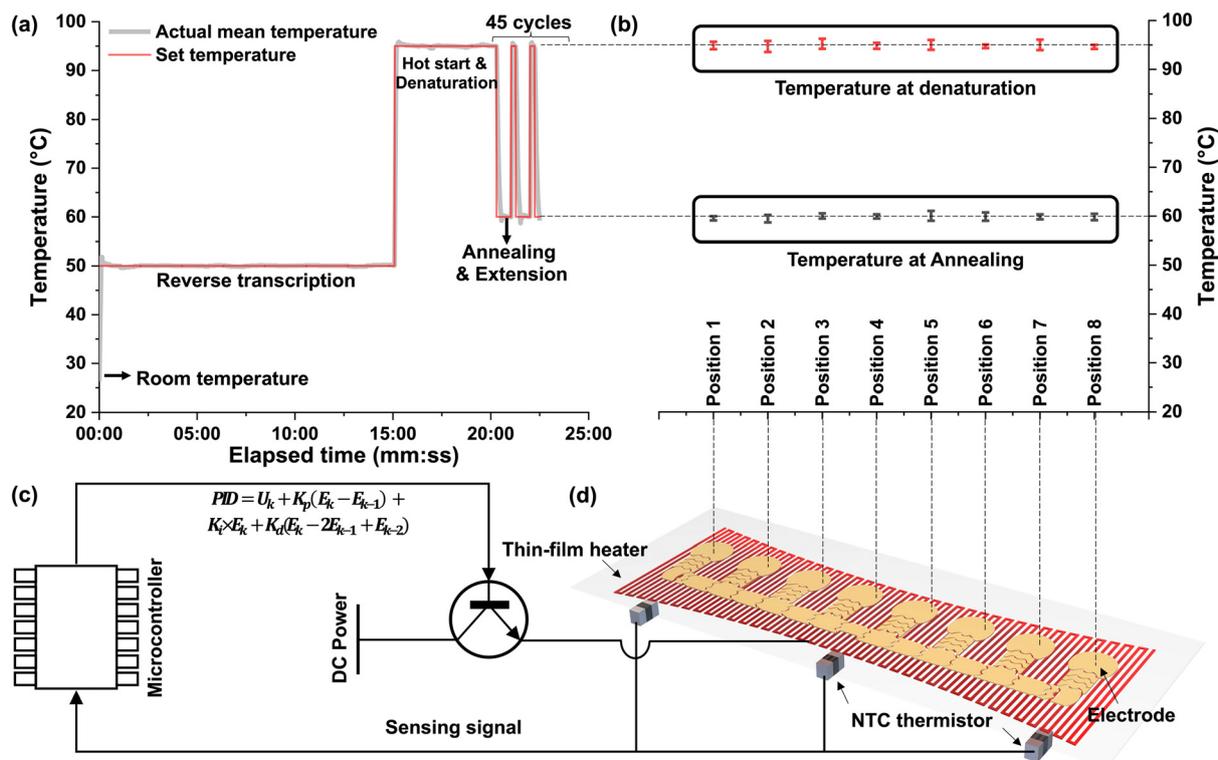
Fig. 2 (a) The set and actual temperature at reaction points on chip during the RT–qPCR process. The mean temperature of eight reaction sites is printed in light grey and the set temperature is printed in red. (b) The temperature at the stable stage of denaturation and annealing by averaging three chips. Error bars are standard deviations of the stable temperatures from these three chips. (c) The thermal control module with the equation of PID control. (d) The 3D explosive diagram of the structure of the chip at reaction sites.

the heating region, some self-compensations were needed to counterbalance the side effects.[30] A serpentine resistor was patterned in an hourglass-shaped geometry (Fig. 2d), while copper foil was configured for a uniform thermal distribution. Traditional thermal loading units were usually built in the device with metal blocks. However, the performance was associated with thermal conductivity, heat capacity, and thermal coupling to the environment of the substrate. The on-chip thin-film heater (heating) and NTC thermistor (sensing) embedded in the PCB were closer to the heating area (*i.e.*, qPCR chamber), making it a short transient regime and quick response by closed-loop control. Therefore, the thermal program was strictly followed for the set temperature with minor discrepancies (Fig. 2a). Despite the heating module being moved onto the chip, the production cost (<2 USD per PCB substrate) is acceptable for disposable use due to the highly developed PCB manufacture. On the other hand, the utilization of on-chip thermal unit miniaturized outline dimensions of the devices, which is beneficial for POCT. Frankly, apart from the contact-based Joule heating, some oncoming technologies are promising and attract interest from many communities, such as surface acoustic waves,[31] microwave[32] and lasers.[33] However, their drawbacks in terms of fabrication, integration, cost, and accuracy of the position and temperature control, *etc.* are evident[34] so far.

Droplet manipulation on macrochannel-to-digital microfluidic platform

In this macrochannel-to-digital platform, 500 μL raw sample underwent nucleic acid extraction through an RNA extraction module; pure RNA was transferred into 60 μL elution buffer at the elution room where the interface of the macrochannel and digital microfluidics is. At the end of the RNA extraction process and the start of the dispensing process, there is a critical interface of the macro-dielectric layer and channel structure, enabling an effective bonding of two patterns of microfluidics. The elution room was entirely situated on the dielectric layer at a height of 1.2 mm, while the height of the paralleled PCB and ITO glass was 0.6 mm. Hence the height difference trapped the elution buffer in this well by surface tension, as shown in Fig. 3a. To actuate the large droplet escaping from the interface, an electrode spanned across the elution room and oil-filled chamber was patterned. Plugging high voltage to adjacent electrodes stepwise could force the eluent to enter into the digital microfluidic controlled region, as shown in Fig. 3b and ESI† video. After the extraction process, the eluent was then actuated to an array of L-shaped electrodes for reaction droplet generation, which is approximately 5.55 μL of each droplet. Their volumes have been determined and discussed in the ESI† (Methods, Results and discussion, and Fig. S3).

The system exhibited eminent stability over a hundred tests of the on-chip "sample-to-answer" workflow. Differing from previous digital-to-microchannel infrastructures, the macrochannel was exploited because it is well-suited for bead-based RNA extraction at a volume of hundreds of microliters. Previous studies combined DMF with microchannel networks by multi-layer design[35] or side-on pattern[36] for handling droplets. However, microchannels could not accommodate large volumes of samples. Meanwhile, the sophisticated structure may introduce more uncertainties which impede their
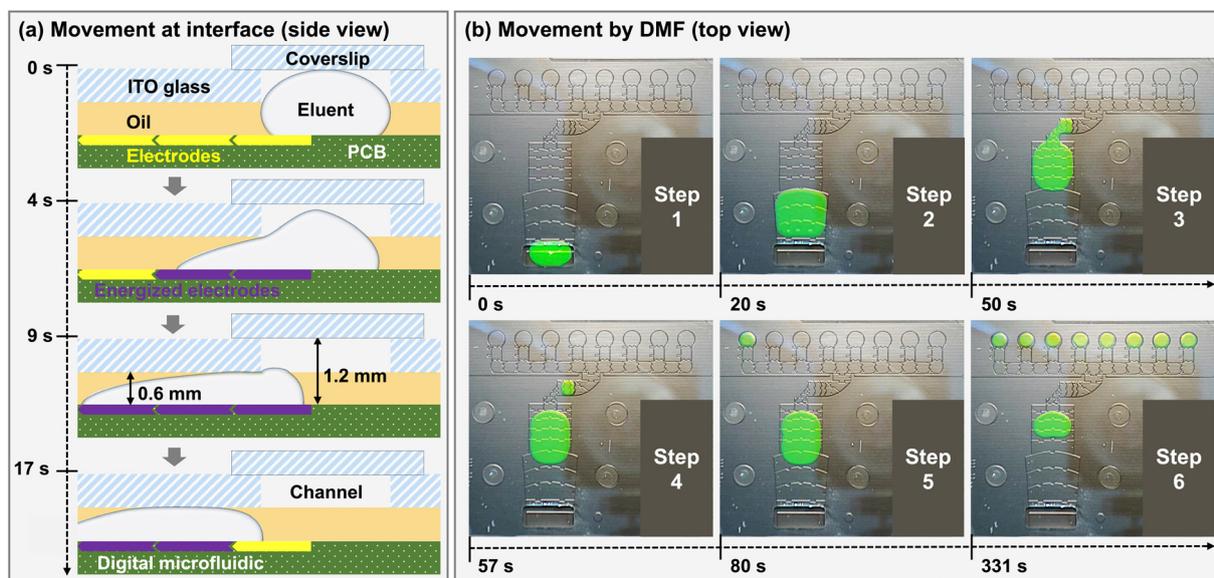
Fig. 3 (a) Illustration (side view) of droplet actuated from macrochannel to digital microfluidic chamber by electrodes. From top to bottom, the figure illustrates (1) the original status of the droplet at the interface of the macrochannel and digital microfluidics. (2) Two electrodes actuate the droplet to overcome surface tension and access the digital microfluidic chamber. (3) The status when three electrodes are active. The heights of the channel and chamber are different. (4) Droplet moves along with the flow of energized electrodes. (b) Series of images from a demo video (top view) depict on-chip droplet movement and dispensing. Steps: (1) droplet emerges in the interface of the macrochannel and digital fluidics. (2) Droplet completely enters the oil-filled chamber and then moves to separating area. (3) Droplet is in the process of dispensing by L-shaped electrodes, then (4–6) transferred to the first and the rest of the qPCR reaction points. For obvious view, saturated calcein (Sigma-Aldrich, US) was hundred times diluted with elution buffer.

commercialization. In contrast, magnetic beads were reported to be compatible with DMF by (1) immobilizing beads and refreshing droplets[37] or (2) extracting and fusing beads with sequential droplets.[38] Herein, a device was developed with the latter mechanism. The released RNA from viruses was adhered to magnetic beads and dragged to sequential cavities for different purposes of treatments, eventually accessing the elution room.

On-chip RNA extraction

The extracted RNA from 10^7 SARS-CoV-2 pseudoviruses through on- and off-chip methods was simultaneously loaded into the qPCR instrument. The cycle thresholds by on-chip extraction were 21.26 ± 0.45 for the N gene and 20.40 ± 0.25 for ORF1 detection, while they are 21.87 ± 0.22 and 21.08 ± 0.38, respectively, extracted by an operator using a commercialized kit (Fig. 4). It has approximately 0.5 difference between N and ORF1 gene detection, though from the same concentration of SARS-CoV-2. This may result from the different amplification efficiency of the two primers and the template sequences. By statistical analysis, on-chip assay could reach the thresholds with less recycles compared to off-chip assays, suggesting that the chip-based extraction performed better than off-chip extraction. Due to the small volume used in the chip, the magnetic beads may adequately come in contact with washing and elution buffers.

Fig. 4 Comparison of the (a) on- and (b) off-chip RNA extraction procedure and (c) results. Error bars are standard deviations from three replicates. The asterisk represents a significant difference between two approaches ($p < 0.01$).

Consequently, chip extracted RNA concentration and/or purity may be slightly higher than that by hand.

On-chip multiplex amplification

For the on-chip amplification module, all pathogenic genes were positively detected at the lowest detected concentration (*i.e.*, 15 copies per test), demonstrating a detection limit likely lower than 15 copies per test. Interestingly, on the fluorescence channel of HEX registration, the ORF1 gene was detected at the lowest cycle threshold among the four channels, which indicates the highest sensitivity of HEX on the device. The off-chip examination exhibited the highest sensitivity on the channel of ROX registration, suggesting that Flu A was the most sensitively detected pathogen in off-chip qPCR devices. Compared with the lower volume (~2 μL) used in the VH 1.0 system, the volume of ~5.55 μL per droplet was believed to increase the detection sensitivity. It was reported that LODs of VH 1.0 were close to 100 copies per test with either LAMP or multiplex qPCR.[27,39] Assuming the RNA concentration in the eluent is 2.7 copies per μL (*i.e.*, 15 copies per test), it has 4.5‰ possibility of taking an empty droplet in 2 μL according to Poisson distribution, which is four orders of magnitude compared with that of the 5.55 μL droplet. Ji *et al.* developed a microfluidic disc-direct RT-qPCR (dirRT-qPCR) assay for rapid multiplex detection of SARS-CoV-2 and influenza A and B viral infection in pharyngeal swab samples. It could detect 20 copies per test of all three pathogens in as little as 2 μL of samples,[40] which are comparable with VH 2.0. However, it should be noted that these LODs were given by actual measurement results without statistical evaluation (*e.g.*, Probit regression). Limited to the sample size (<20 reactions), LOD was also farfetched in this section and for off-chip complete workflow (in the next section); thus, they were not presented.

Meanwhile, the low inter-assay and intra-assay variations (<5.00%, data not shown) demonstrated the homogeneity and reproducibility of the amplification module, which may be attributed to the uniformity of the droplet volume and the subtle thermal actuation unit. In addition, both on- and off-chip amplification have a high correlation coefficient (R^2 >0.99, Table 1). The high linearity of amplification is prerequisite for quantitation and high sensitivity of integrated chips. Meanwhile, the linearity (*i.e.*, R^2) of on-chip amplification performed comparably with that of off-chip amplification indicated by two-tailed Student *t*-test coefficient, $p = 0.13 > 0.05$. Without manual intervention, the stochastic error induced by users' operation was minimized. The volumes of the on-chip droplets were measured based on the documented method[41] (detailed in the ESI†). The digital microfluidics exhibited inherent superiority in precisely manipulating tiny droplets (*i.e.*, droplet splitting and moving), conferring the stable performance of the RT-qPCR.
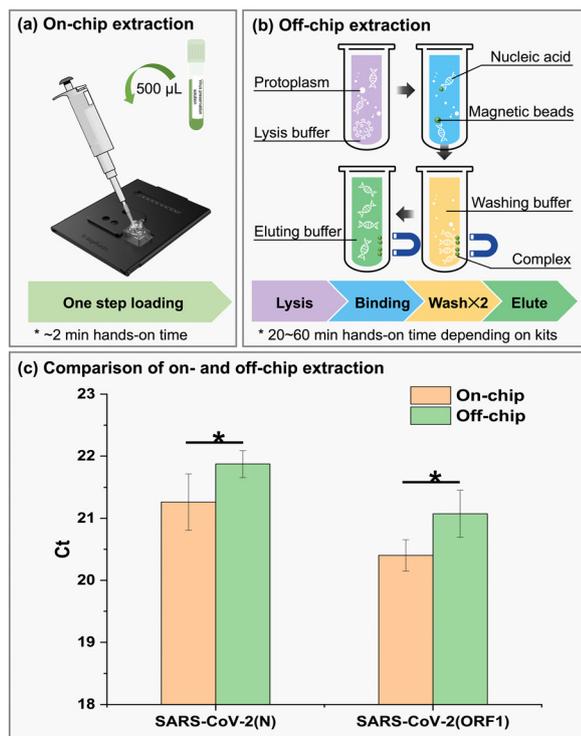
Performance of VH 2.0 integrated platform

To evaluate the performance of integrated chips, series concentrations of pseudoviruses were tested and the limit of

Table 1 Comparisons of linearity of on-chip and off-chip amplification process for various pathogens

Target	Standard curve	R^2	Mean Ct of 15 copies/T	CV of 15 copies/T (%)	Detection rate
On-chip					
Flu A	$y = -3.00x + 39.44$	0.971^a	35.60	0.37	16/16
Flu B	$y = -2.91x + 36.61$	0.994	33.16	2.41	16/16
SARS-CoV-2(N)	$y = -3.52x + 41.25$	0.991	36.94	3.54	16/16
SARS-CoV-2(ORF1)	$y = -3.18x + 32.57$	0.996	28.85	0.25	16/16
Off-chip					
Flu A	$y = -4.09x + 32.28$	0.990	27.68	4.54	20/20
Flu B	$y = -3.99x + 35.28$	0.990	30.76	4.33	20/20
SARS-CoV-2(N)	$y = -4.17x + 39.15$	0.994	34.25	3.72	19/20
SARS-CoV-2(ORF1)	$y = -4.11x + 39.46$	0.993	34.56	1.79	19/20

^{a} It could be 0.999 if the curve does not include the lowest concentration. The negative controls (sample without template) did not acquire Ct values.

detection with 95% detection possibility (LOD_{95}) was estimated by Probit regression (derived from >40 reactions). Same as the amplification module of the chip, the integrated chip also exhibited a high linearity (Table 2), illustrating the robustness of the extraction module as well as the whole chip. Both on-chip and off-chip detection could be linearly fitted with a coefficient of determination R^2 higher than 0.99. The HEX registered the highest sensitivity among four fluorescence channels; therefore, the LOD_{95} of SARS-CoV-2 (ORF1) could achieve 302 copies per mL. Other pathogens can be stably detected as low as approximately 1000 copies per mL. The numbered test counts were all positively detected by an off-chip qPCR instrument, resulting in the non-deducible LOD_{95}. However, they were most likely lower than the minimum detected concentrations (*i.e.*, 1000 copies per mL for Flu B/ORF1/N and 100 copies per mL for Flu A). The LOD for integrated chip assay was conspicuously lower than that of amplification parts. Such a discrepancy was caused by integration of the extraction process, which inevitably led to the loss of nucleoid acid. Moreover, the impurities from samples or extraction reagents may also inhibit the amplification.[42] The qPCR efficiencies ranged from 100% to 110% on-chip, while the off-chip assays varied from 94% to 97%. Fluorescence was not detected from any negative samples (derived from preservation solution) and samples spiked with other pathogens that were not the target of detection, declaring the high specificity of integrated chips.

PCR efficiency is the fraction of target molecules that are copied in one cycle, which is an important indicator of the quantitative process. Results showed that the values were all within the widely accepted range (*i.e.*, 90–110%) that is recommended for qPCR reactions.[43] Typically, efficiency is significantly impacted by the instruments, replicates, and concentrations used for standard curve generation.[44] A total of 72 reactions in 9 independent chips for at least 5 concentrations were performed in this research, guaranteeing the reliability of the evaluation. Thus, in our experiment, the differences between on- and off-chip tests may be largely contributed by different instruments.

Performance in clinical application

Eleven SARS-CoV-2 and Flu A positive clinical specimens and four negative specimens from healthy people were tested. Results show a 100% coincidence between on- and off-chip assays for these two pathogen detection. Considering the satisfactory performances of the chip in detecting pseudoviruses, the Ct values measured by on- and off-chip methods presented a strong positive correlation as expected (Fig. 5 and Table S3†), especially for Flu A and ORF1 gene detection. The Pearson's coefficients were both higher than 0.9 with p values lower than 0.01. The N gene detection was a little off but the p value was low as well (0.0002), indicating the positive correlation between on- and off-assays is

Table 2 Summary of on-chip and off-chip whole process performance

Target	Standard curve	Linear range (copies per mL)	R^2	Efficiency (%)	LOD_{95} (copies per mL)
On-chip					
Flu A	$y = -3.10x + 43.54$	10^2–10^6	0.996	110	1027.19
Flu B	$y = -3.20x + 43.90$	10^2–10^6	0.995	106	1258.11
SARS-CoV-2(N)	$y = -3.31x + 42.56$	10^2–10^6	0.989^a	100	943.91
SARS-CoV-2(ORF1)	$y = -3.24x + 40.01$	10^2–10^7	0.991	104	302.22
Off-chip					
Flu A	$y = -3.48x + 46.16$	10^3–10^6	1.000	94	NA
Flu B	$y = -3.47x + 49.24$	10^2–10^6	0.996	94	NA
SARS-CoV-2(N)	$y = -3.42x + 44.22$	10^3–10^7	0.993	96	NA
SARS-CoV-2(ORF1)	$y = -3.40x + 45.23$	10^2–10^7	0.994	97	NA

NA: not available. ^{a} The coefficient of determination R^2 lower than 0.99 was marked.
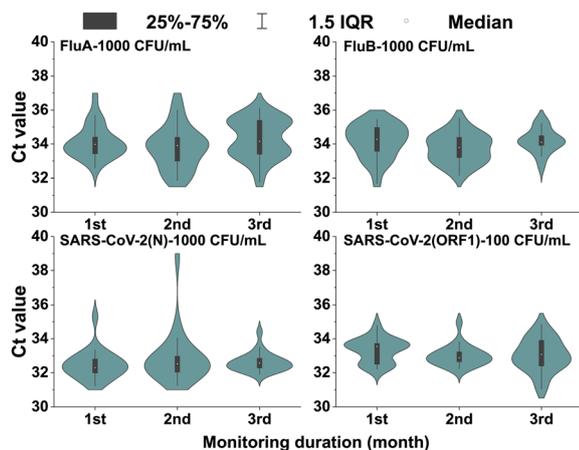
Fig. 5 The violin plot of Ct values during the stability assay. The medians (hollow circle), 1.5 interquartile ranges (whisker), upper and lower quartiles (box), and data distribution patterns (violin outline) are presented accordingly.

convincing. Numbered clinical specimens ineludibly introduced bias that may not cover all the possibilities, for instance, the weakly positive samples may be challenging for detection. The lowest pathogen load among tested samples appeared in No. 11 Flu A specimen (Table S4†), which was reported as 36.07 by VH 2.0. Also, the Ct value of No. 10 Flu A specimen was 35.11 which is close to the LOD_{95} (the corresponding Ct is 34.20). These two clinical samples were probabilistic detected by chip (7/8). Thanks to the eight parallel reaction models on chip, the possibilities of misdiagnosis were reduced. For SARS-CoV-2, the detection of two specific genes can double verify the accuracy of the results. Thus, the chip leads to a robust and convincing result in clinical applications.

The stability of VH 2.0 biochips

Concentrations near the LOD_{95} were selected for stability assay. VH 2.0 biochips (with all reagents prestored) exhibited relatively stable Ct values at all registered fluorescence channels (Fig. 5), which were 34.09 ± 0.26 for Flu A, 34.03 ± 0.24 for Flu B, 32.64 ± 0.20 for SARS-CoV-2(N), and 33.12 ± 0.19 for SARS-CoV-2(ORF1). It demonstrated that the detection of Flu A/B and SARS-CoV-2 (ORF1/N) was reproducible and the chips were stable within the three-month monitoring duration. Although a slight fluctuation of Ct values was observed during the 3 months, the differences were statistically insignificant according to Student's t-test. All p-values within the cohort were greater than 0.05 (Table S5†). Also, the intra-assay CVs were in the range from 1.72% to 4.70% and inter-assay CVs were around 0.7%. Both were consistently acceptable (less than 5%) under various conditions.

The stability assay is an essential step for scaling up the products. Ideally, the long-term stability test should be conducted on the day of product deterioration, demonstrating

availability within the shelf-life. However, due to time constraints, only three months were monitored after the date of manufacture. Indeed, the stability of the chip includes the stability of all the reagents, filled oil, encapsulation, lifetime of the coating and electronics on the chips. To guarantee the superior performance of the products, a stability test report for each component was acquired from suppliers based on their qualified assays. On the other hand, we made many attempts to improve the stability during the fabrication, such as the reagent dehydration technology, brand of oil, sealing technology, *etc.* The DMF chips can be stably used under practical conditions for more than 1 year according to the first-generation product.

Comparison with existing platforms

The pandemic caused by SARS-CoV-2 has not only upended the daily lives of billions but also changed the diagnostic landscape. NATs have partially replaced conventional culture and antigen detection assays because of their capability of fast and accurate detection. A number of commercialized NAT-based platforms have been developed for identifying respiratory pathogens. Here, the VH 2.0 system was comprehensively compared with 9 POCT platforms, 16 panels including 9 US FDA-cleared or EUA respiratory panels, 3 previous versions of our product, 2 representative respiratory panels, and 2 panels developed by research groups (Table 3).

The chosen platforms were reported to be able to detect 1–23 respiratory pathogens in a single detection. Multiplex RT-qPCR as one of the most developed technologies has been widely used for routine diagnostic applications. However, limited by the number of fluorophores (typically 4 or 5 channels), only several targets can be detected per reaction. Thus, tagging oligonucleotide cleavage and extension (TOCE), dual priming oligonucleotide (DPO), and multiplex ligation-dependent probe amplification (MLPA) were developed to overcome such limitations by specially designed primers and probes. These technologies have been implemented in the products of Seegene such as SeeplexII RV15 and AnyplexII RV 16.[45] However, the sophisticated primer and probe need experienced users and results have to be analysed by bundled software. Notably, microfluidic technology combined with RT-qPCR is an alternative methodology to increase the detection targets. In detail, DMF technology is propitious to generate many droplets. Combined with multiplex qPCR, the detection targets can be multiplied. As listed in Table 3, our DMF systems, Onestart from Baicare and a platform from Kansas State University adopted DMF plus multiplex qPCR as a basic principle. Apart from these, DMF is also compatible with other nucleic acid probing technologies, such as eSensor™[46,47] from GenMark and recombinase polymerase amplification (RPA) coupled with DETECTR[48] adopted by the RCD platform. Among them, eSensor™ relies on competitive DNA hybridization and electrochemical detection. It has been successfully commercialized, and its Respiratory Pathogen Panel 2 was authorized for emergency use by the US Food & Drug

Table 3 The comparisons with existing platforms

Manufacturer	Platform (device)	Panel (chip or cartridge)	Methodology	Targets	Turnaround time (min)	Throughput	NA extraction integrated	NA FDA authorized	Sensitivity (%)	Specificity (%)	Ref.
Digifluidic Biotech	VH 2.0	RP panel v3	DMF + multiplex RT-qPCR	3 (max. 32)	120	1–10	Yes	No	100	100.0	This research
	VH 1.0	RP panel v1		4	90		No		94.0	100.0	52
		RP panel v2		11					93.3	100.0	39
		Foodborne pathogens	DMF + LAMP	4	30				—	—	27
Cepheid	GeneXpert	CoV-2 plus	MF + multiplex RT-qPCR	1	20–30	1–80	Yes	EUA	95.2	95.0	53
		CoV-2/Flu/RSV plus		3	45			Yes	100.0	98.3	
BioFire Diagnostics	Torch	RP panel	Nest-PCR-endpoint melt curve analysis	21	60	1–12	Yes	Yes	84.5–97.9	96.1–100	54
		RP 2.1 plus panel		23	45				97.1	99.3	55
	SPOTFIRE	R panel		15	15	1–4			96.3–100	90.6–100	56
GenMark Dx	ePlex	RP panel	DMF + voltammetry	20	90	3–24	No[a]	Yes	95.4	99.7	54 and 57
		RP panel 2		21			Yes	EUA	91.4–98.3	99.2–99.7	57 and 58
Luminex Molecular Diagnostics	MAGPIX	xTAG RVP v1	Fluorescence-labeled bead array + cytometry	20	240	1–96	No	Yes	87.2–91.2	99.7–100	54 and 59
		xTAG RVP fast v2		19					78.8–92	97–99.6	54 and 60
Baicare Biotechnology	Onestart	RP panel	DMF + monoplex RT-qPCR	21	90	1	Yes	No	—	100.0	61
Kansas State University	—	SARS-CoV-2	DMF + multiplex RT-qPCR	1	17/42	1	No	—	—	—	62
Xiamen University	RCD	RP panel	PRA + Cas12a	2	30	1	No	—	100	100	63

RV: respiratory viruses; RP: respiratory pathogens; FDA: Food and Drug Administration; EUA: emergency use authorization. [a] Need to pipet 200 µL of the sample to the sample delivery device and vortex for 10 s.

Administration (FDA) in 2020.[49] However, both methods have their pros and cons. Due to electrochemistry utilizing molecular hybridization without amplification, it is capable of miniaturizing the device, reducing the risk of aerosol contamination, and enhancing the specificity; nevertheless, the most severe limitation is the detection limit, which is far below that of fluorometric assays.[50] On the other hand, isothermal amplification such as real-time loop-mediated isothermal amplification (LAMP) and RPA dramatically shorten the reaction time while simplifying the structure of the heating module, whereas its sensitivity and specificity cannot be compared with qPCR[51] and it is challenging for either primer design or absolute quantification. In addition to DMF, channel-based microfluidics (CMF) has been employed by GeneXpert from Cepheid and FilmArray from BioFire Diagnostics. CMF requires extra pumps or valves to control fluid, leading to a higher cost for each diagnosis compared with DMF.

The VH 2.0 instrument mounted 4 fluorescence channels and the tailor-made chip has 8 reaction rooms, resulting in the theoretical detection capacity reaching 32 targets. Further, the self-developed lysis buffer was designed for both viruses and bacteria, allowing the detection target to be expanded to infectious bacteria, such as *S. pneumoniae*, *H. influenzae*, *S. aureus*, *S. enterica*, and *S. flexneri*, which could be lysed by the buffer. Globally, evidence shows the flexibility and feasibility of DMF for detecting multiple pathogens.

The single run time of RP v3 of Digifluidic Biotech is approximately 2 h, which is relatively longer than that of other panels. It results from two reasons: (1) the prestored reagents are incompatible with fast PCR which mainly depends on the efficiency of enzymes; (2) lower power was selected for stable thermal control and matching with present PCR reagents. Unremitting efforts are made to shorten the turnaround time such as the development of fast/extreme qPCR, corresponding reagents, and improvement of the thermal module. To meet the requirements of point-of-care testing, VH 2.0 was designed as an independent cartridge integrating a nucleic acid extraction process on the chip as GeneXpert, FilmArray, and Onestart do. All the reagents required by extraction and reaction have been prestored in the corresponding cavities, thereby no extra pipetting is needed. Compared to VH 1.0, such update greatly shortened the hands-on time and simplified the diagnosis, lifting the need for experienced operators. Although batchwise testing systems (*e.g.*, BD Viper™ XTR/LT system, Cobas® 4800/6800/8800 system, *etc.*) automatically possess high throughput per analysis station, these systems are costly and have large footprints which constrain scale-up testing and deployment in low-resource settings for mass screening. Coincidentally, portable all-in-one POCT devices such as VH 2.0 complement batchwise systems.

Conclusions

This study developed an all-in-one diagnostic platform based on a macrochannel-to-digital microfluidic platform for automatic identification of multiple viruses. The special designs for on-chip thermal control and hybrid microfluidics enable stability and ease of fabrication. PCB and prefabricated blocks were employed for chip construction, which can reduce the cost and rejection rate during mass production. It is therefore beneficial to product commercialization. This research involved three respiratory pathogens (*i.e.*, SARS-CoV-2, Flu A, and Flu B) for a proof-of-concept study. Through comprehensive evaluations, this platform exhibited a stable performance for its extraction, amplification modules, and sample-to-answer process. Notably, its sensitivity, specificity, detection limit, and amplification efficiency are comparable to that of the off-chip RT-qPCR process. The platform could easily extend to a maximum of 32 targets by simply changing the primers and probes. Furthermore, the platform dramatically reduces the hands-on time and the professional requirements of operators and equipment compared with traditional PCR. Overall, this research made certain academic and application merits for DMF in the field of diagnosis.

Author contributions

Conceptualization and methodology: Dr. Cheng Dong, Dr. Tianlan Chen, Dr. Fei Li. Investigation, formal analysis, and writing – original draft: Yun Sun, Dr. Fei Li. Visualization: Dr. Fei Li, Dr. Chunzhao Chen, Dr. Cheng Dong. Funding acquisition, project administration, and resources: Dr. Tianlan Chen, Dr. Cheng Dong, Dr. Rui P. Martins, Dr. Pui-In Mak, Dongling Long. All authors were involved in writing – review & editing.

Conflicts of interest

There are no conflicts to declare.

Acknowledgements

Notes and references

1 R. Wölfel, V. M. Corman, W. Guggemos, M. Seilmaier, S. Zange, M. A. Müller, D. Niemeyer, T. C. Jones, P. Vollmar and C. Rothe, *Nature*, 2020, **581**, 465–469.

2 Z. Ballard and A. Ozcan, *Nat. Biomed. Eng.*, 2018, **2**, 629–630.

3 K. J. Cortez, E. Roilides, F. Quiroz-Telles, J. Meletiadis, C. Antachopoulos, T. Knudsen, W. Buchanan, J. Milanovich, D. A. Sutton, A. Fothergill, M. G. Rinaldi, Y. R. Shea, T. Zaoutis, S. Kottilil and T. J. Walsh, *Clin. Microbiol. Rev.*, 2008, **21**, 157–197.

4   C. A. Muzny, R. J. Blackburn, R. J. Sinsky, E. L. Austin and J. R. Schwebke, *Clin. Infect. Dis.*, 2014, **59**, 834–841.

5   S. Zayet, N. d. J. Kadiane-Oussou, Q. Lepiller, H. Zahra, P.-Y. Royer, L. Toko, V. Gendrin and T. Klopfenstein, *Microbes Infect.*, 2020, **22**, 481–488.

6   C. Rothe, M. Schunk, P. Sothmann, G. Bretzel, G. Froeschl, C. Wallrauch, T. Zimmer, V. Thiel, C. Janke and W. Guggemos, *N. Engl. J. Med.*, 2020, **382**, 970–971.

7   Center for Systems Science and Engineering, *COVID-19 dashboard*, Center for Systems Science and Engineering at Johns Hopkins University, 2023, **https://coronavirus.jhu.edu**.

8   J. Zhao, Q. Yuan, H. Wang, W. Liu, X. Liao, Y. Su, X. Wang, J. Yuan, T. Li and J. Li, *Clin. Infect. Dis.*, 2020, **71**, 2027–2034.

9   K. Choi, A. H. Ng, R. Fobel and A. R. Wheeler, *Annu. Rev. Anal. Chem.*, 2012, **5**, 413–440.

10 M. Washizu, *IEEE Trans. Ind. Appl.*, 1998, **34**, 732–737.

11 Q. Zhang, X. Xu, L. Lin, J. Yang, X. Na, X. Chen, L. Wu, J. Song and C. Yang, *Lab Chip*, 2022, **22**, 1971–1979.

12 X. Xu, L. Lin, J. Yang, W. Qian, R. Su, X. Guo, L. Cai, Z. Zhao, J. Song and C. Yang, *Nano Today*, 2022, **46**, 101596.

13 J. Lamanna, E. Y. Scott, H. S. Edwards, M. D. Chamberlain, M. D. M. Dryden, J. Peng, B. Mair, A. Lee, C. Chan, A. A. Sklavounos, A. Heffernan, F. Abbas, C. Lam, M. E. Olson, J. Moffat and A. R. Wheeler, *Nat. Commun.*, 2020, **11**, 5632.

14 A. Das, C. Weise, M. Polack, R. D. Urban, B. Krafft, S. Hasan, H. Westphal, R. Warias, S. Schmidt, T. Gulder and D. Belder, *J. Am. Chem. Soc.*, 2022, **144**, 10353–10360.

15 W. Qiu and S. Nagl, *ACS Sens.*, 2021, **6**, 1147–1156.

16 S. Han, Q. Zhang, X. Zhang, X. Liu, L. Lu, J. Wei, Y. Li, Y. Wang and G. Zheng, *Biosens. Bioelectron.*, 2019, **143**, 111597.

17 S. Battat, D. A. Weitz and G. M. Whitesides, *Lab Chip*, 2022, **22**, 530–536.

18 R. Shen, S. Yi, P. Wang, P.-I. Mak, R. P. Martins and Y. Jia, *TrAC, Trends Anal. Chem.*, 2022, 116826.

19 J. Li and C.-J. C. Kim, *Lab Chip*, 2020, **20**, 1705–1712.

20 Y. Xing, Y. Liu, R. Chen, Y. Li, C. Zhang, Y. Jiang, Y. Lu, B. Lin, P. Chen, R. Tian, X. Liu and X. Cheng, *Lab Chip*, 2021, **21**, 1886–1896.

21 R. Shen, Y. Jia, P.-I. Mak and R. P. Martins, *Lab Chip*, 2020, **20**, 1928–1938.

22 J. Li, N. S. Ha, T. L. Liu, R. M. van Dam and C.-J. 'Cj' Kim, *Nature*, 2019, **572**, 507–510.

23 T.-W. Huang, T.-Y. Ho and K. Chakrabarty, Reliability-oriented broadcast electrode-addressing for pin-constrained digital microfluidic biochips, in *2011 IEEE/ACM International Conference on Computer-Aided Design (ICCAD)*, IEEE, 2011, pp. 448–455.

24 Z. Li, T. A. Dinh, T.-Y. Ho and K. Chakrabarty, Reliability-driven pipelined scan-like testing of digital microfluidic biochips, in *2014 IEEE 23rd Asian Test Symposium*, IEEE, 2014, pp. 57–62.

25 S.-J. Wang, K. S.-M. Li and T.-Y. Ho, Design-for-Reliability and Probability-Based Fault Tolerance for Paper-Based Digital Microfluidic Biochips with Multiple Faults, in *2022 27th Asia and South Pacific Design Automation Conference (ASP-DAC)*, IEEE, 2022, pp. 62–67.

26 Y. Zai, C. Min, Z. Wang, Y. Ding, H. Zhao, E. Su and N. He, *Lab Chip*, 2022, **22**, 3436–3452.

27 M. Xie, T. Chen, X. Xin, Z. Cai, C. Dong and B. Lei, *Food Control*, 2022, **136**, 108824.

28 V. Luu-The, N. Paquet, E. Calvo and J. Cumps, *BioTechniques*, 2005, **38**, 287–293.

29 J. Pierson-Perry, J. Vaks, A. Durham, C. Fischer, C. Gutenbrunner, D. Hillyard, M. Kondratovich, P. Ladwig and R. Middleberg, *Evaluation of Detection Capability for Clinical Laboratory Measurement Procedures*, Clinical and Laboratory Standards Institute, Wayne, PA, USA, 2nd edn, 2012.

30 T.-M. Hsieh, C.-H. Luo, F.-C. Huang, J.-H. Wang, L.-J. Chien and G.-B. Lee, *Sens. Actuators, B*, 2008, **130**, 848–856.

31 R. J. Shilton, V. Mattoli, M. Travagliati, M. Agostini, A. Desii, F. Beltram and M. Cecchini, *Adv. Funct. Mater.*, 2015, **25**, 5895–5901.

32 T. Markovic, S. Liu, I. Ocket and B. K. J. C. Nauwelaers, *Int. J. Microw. Wirel. Technol.*, 2017, **9**, 1591–1596.

33 H. Kim, S. Vishniakou and G. W. Faris, *Lab Chip*, 2009, **9**, 1230–1235.

34 V. Miralles, A. Huerre, F. Malloggi and M.-C. Jullien, *Diagnostics*, 2013, **3**, 33–67.

35 M. Abdelgawad, M. W. L. Watson and A. R. Wheeler, *Lab Chip*, 2009, **9**, 1046–1051.

36 G. Sathyanarayanan, M. Haapala, C. Dixon, A. R. Wheeler and T. M. Sikanen, *Adv. Mater. Technol.*, 2020, **5**, 2000451.

37 Y. Fouillet, D. Jary, C. Chabrol, P. Claustre and C. Peponnet, *Microfluid. Nanofluid.*, 2008, **4**, 159–165.

38 M. Shikida, K. Takayanagi, K. Inouchi, H. Honda and K. Sato, *Sens. Actuators, B*, 2006, **113**, 563–569.

39 H. Huang, K. Huang, Y. Sun, D. Luo, M. Wang, T. Chen, M. Li, J. Duan, L. Huang and C. Dong, *Micromachines*, 2022, **13**, 1650.

40 M. Ji, Y. Xia, J. F.-C. Loo, L. Li, H.-P. Ho, J. He and D. Gu, *RSC Adv.*, 2020, **10**, 34088–34098.

41 M. J. Kiani, A. Dehghan, M. Saadatbakhsh, S. J. Asl, N. M. Nouri and E. Pishbin, *Lab Chip*, 2023, **23**(4), 748–760.

42 I. G. Wilson, *Appl. Environ. Microbiol.*, 1997, **63**, 3741–3751.

43 J. Ruijter, C. Ramakers, W. Hoogaars, Y. Karlen, O. Bakker, M. Van den Hoff and A. Moorman, *Nucleic Acids Res.*, 2009, **37**, e45.

44 D. Svec, A. Tichopad, V. Novosadova, M. W. Pfaffl and M. Kubista, *Biomol. Detect. Quantif.*, 2015, **3**, 9–16.

45 C. H. Cho, B. Chulten, C. K. Lee, M. H. Nam, S. Y. Yoon, C. S. Lim, Y. Cho and Y. K. Kim, *J. Clin. Virol.*, 2013, **57**, 338–342.

46 S. D. Vernon, D. H. Farkas, E. R. Unger, V. Chan, D. L. Miller, Y.-P. Chen, G. F. Blackburn and W. C. Reeves, *BMC Infect. Dis.*, 2003, **3**, 12.

47 J. E. Schmitz and Y.-W. Tang, *Future Microbiol.*, 2018, **13**, 1697–1708.

48 J. S. Chen, E. Ma, L. B. Harrington, M. Da Costa, X. Tian, J. M. Palefsky and J. A. Doudna, *Science*, 2018, **360**, 436–439.

49   *ePlex Respiratory Pathogen Panel 2 - Letter of Authorization*, US Food & Drug Administration, 2020, **https://www.fda.gov/media/142902/download#:~:text=This%20test%20is%20only%20authorized,and%20Cosmetic%20Act%2C%2021%20U.S.C.**

50   M. Lazerges and F. Bedioui, *Anal. Bioanal. Chem.*, 2013, **405**, 3705–3714.

51   J. Song, C. Liu, M. G. Mauk, S. C. Rankin, J. B. Lok, R. M. Greenberg and H. H. Bau, *Clin. Chem.*, 2017, **63**, 714–722.

52   W. Li, X. Jiang, H. Wang, M. Wang, A. Zhou, D. Luo, T. Chen and C. Dong, *J. Trop. Med.*, 2022, **22**, 1487–1492.

53   L. D. Noble, L. E. Scott, R. Munir, M. Du Plessis, K. Steegen, L. Hans, P. Marokane, P. Da Silva and W. S. Stevens, *Diagnostics*, 2022, **13**, 34.

54   E. B. Popowitch, S. S. O'Neill and M. B. Miller, *J. Clin. Microbiol.*, 2013, **51**, 1528–1533.

55   bioMérieux, *BIOFIRE® Respiratory 2.1 plus Panel*, **https://www.biomerieux-diagnostics.com/biofirer-respiratory-21-plus-panel**.

56   US FDA, *510(k) Premarket Notification of BIOFIRE SPOTFIRE Respiratory (R) Panel*, 2023, **https://www.accessdata.fda.gov/scripts/cdrh/cfdocs/cfpmn/pmn.cfm?ID=K213954**.

57   J. Jarrett, K. Uhteg, M. S. Forman, A. Hanlon, C. Vargas, K. C. Carroll, A. Valsamakis and H. H. Mostafa, *J. Clin. Virol.*, 2021, **135**, 104737.

58   W. Zhen, E. Smith, R. Manji, D. Schron and G. J. Berry, *J. Clin. Microbiol.*, 2020, **58**, e00783-20.

59   H.-K. Kim, S.-H. Oh, K. A. Yun, H. Sung and M.-N. Kim, *J. Clin. Microbiol.*, 2013, **51**, 1137–1141.

60   Luminex Corporation, *xTAG® Respiratory Viral Panel (RVP) FAST v2*, 2012, **https://www.ld.ru/w/multiplex/RVP-FAST-v2-Brochure.pdf**.

61   E. Huang, Y. Wang, N. Yang, B. Shu, G. Zhang and D. Liu, *Anal. Bioanal. Chem.*, 2021, **413**, 1787–1798.

62   K.-L. Ho, H.-Y. Liao, H. M. Liu, Y.-W. Lu, P.-K. Yeh, J. Y. Chang and S.-K. Fan, *Micromachines*, 2022, **13**, 196.

63   Z. Sun, K.-F. Lin, Z.-H. Zhao, Y. Wang, X.-X. Hong, J.-G. Guo, Q.-Y. Ruan, L.-Y. Lu, X. Li, R. Zhang, C.-Y. Yang and B.-A. Li, *Sci. China: Chem.*, 2022, **65**, 630–640.